Master's Thesis
석사 학위논문

Fabrication Process of High Performance Organic Photodiode Array for Full Color Imaging

Kyu Min Sim (심 규 민 沁 揆 民)

Department of
Energy Science & Engineering

DGIST

2020

Master's Thesis
석사 학위논문

Fabrication Process of High Performance Organic Photodiode Array for Full Color Imaging

Kyu Min Sim (심 규 민 沁 揆 民)

Department of
Energy Science & Engineering

DGIST

2020

Fabrication Process of High Performance Organic Photodiode Array for Full Color Imaging

Advisor: Professor Jiwoong Yang
Co-advisor: Professor Jongmin Choi

by

Kyu Min Sim
Department of Energy Science & Engineering
DGIST

A thesis submitted to the faculty of DGIST in partial fulfillment of the requirements for the degree of Master of Science in the Department of Energy Science & Engineering. The study was conducted in accordance with Code of Research Ethics[1]

05. 08. 2020

Approved by

Professor Jiwoong Yang (signature)
(Advisor)

Professor Jongmin Choi (signature)
(Co-Advisor)

[1] Declaration of Ethical Conduct in Research: I, as a graduate student of DGIST, hereby declare that I have not committed any acts that may damage the credibility of my research. These include, but are not limited to: falsification, thesis written by someone else, distortion of research findings or plagiarism. I affirm that my thesis contains honest conclusions based on my own careful research under the guidance of my thesis advisor.

Fabrication Process of High Performance Organic Photodiode Array for Full Color Imaging

Kyu Min Sim

Accepted in partial fulfillment of the requirements for the degree of Master of Science.

05. 08. 2020

Head of Committee Prof. Jiwoong Yang (signature)

Committee Member Prof. Jongmin Choi (signature)

Committee Member Prof. Ju-Hyuck Lee (signature)

MS/ES
201744001

심 규 민. Kyu Min Sim. Fabrication Process of High Performance Organic Photodiode Array for Full Color Imaging. Department of Energy Science & Engineering. 2020. 55p. Advisors Prof. Jiwoong Yang, Co-Advisors Prof. Jongmin Choi

ABSTRACT

As interest in applications in biomedicine, education, environmental monitoring, optical communications, pharmaceutics and machine vision grows, interest in image sensors are growing. However, in order to apply the image sensor to various applications, there are many limitations such as the thick thickness of Si (>3 ㎛), the need for color filters for the color selectivity, and insufficient mechanical properties. Organic semiconductors are a very attractive material to cover these problems. In this paper, we present the mechanism and manufacturing process of color-selective photodiode using organic semiconductor.

Keywords: Organic image sensor, Organic photodiode, Organic semiconductor, Patterning process

List of Contents

Abstract ····· i

List of contents ····· ii

List of tables ····· iii

List of figures ····· vi

Part 1.

1.1 ····· 8

1.2 ····· 10

1.3 ····· 21

Part 2.

2.1 ····· 31

2.2 ····· 33

2.3 ····· 47

Part 1. Facile tuning the detection spectrum of Organic Thin Film Photodiode via Selective Exciton Activation

I. INTRODUCTION

The ability to accurately detect color and intensity of light is a key role of an image sensor used for video application and machine vision. In particular, in order to detect color with high precision, it is very important to use a photodiode with narrow band detection ability with narrow full width at half maximum. [1,2] Due to the broadband absorption characteristic of Si, commonly used Si-CMOS image sensors use R/G/B color filters combined with Si photodiode to realize narrow band detection. This approach increases the complexity of image sensor, and thus, not only limits integrity but also increases the fabrication cost. Moreover, due to the low extinction coefficient of Si, a thick film of thickness ≈3 μm is required to absorb sufficient light for photodiode operation, resulting in an increased probability of inter-pixel cross-talk, which eventually limits the resolution of the image sensor. [2-4] To overcome these drawbacks of Si photodiode, organic photodiodes (OPDs) have been intensively developed for the last decade. Contrary to the case of Si with indirect bandgap, organic semiconductors with direct highest occupied molecular orbital–lowest unoccupied molecular orbital transition have high extinction coefficient, and thus, they can better absorb the illuminated light with thickness as small as few hundreds of nanometers. In addition, the absorption spectrum of organic semiconductor can be controlled by adjusting the conjugation length, which opens up the possibility of full color detection without a color filter. Furthermore, as the organics have low weight, flexibility, and solubility in organic solvent, it can be used in a variety of

applications. [1,3] Therefore, over the past decade, R/G/B-selective OPDs have been developed through the smart combination of narrow-band absorption materials with various device architectures. Lim and coworkers utilized donor-acceptor copolymers with green-selective absorption spectrum to fabricate high detectivity (D*) bulk heterojunction (BHJ) and thin-film green-selective OPDs. [5] Chung and coworkers devised both blue- and green-selective thin-film OPDs by respectively using the blue- and green- selective organic semiconductors as donors and non-absorbing oxide semiconductors as acceptors with planar heterojunction geometry. [6,7] However, realizing the red-selective OPD by using the synthesis technology of the organic semiconductor alone is difficult. This is due to the difficulty of confining the π-conjugated structure only to the 635 nm region, which usually corresponds to band I absorption of low-bandgap polymers. To solve this problem, optical manipulation method such as charge collection narrowing method (CCN) was demonstrated by Armin and coworkers to realize narrow-band red-selective OPDs with detectivity reaching 2×10^{12} Jones. [8] However, this strategy has the limitation of an active layer thickness exceeding 1.5 μm while realizing the narrow-band detection, resulting in Si-like active layer thickness.

In this article, we propose a method of realizing R/G/B full-color detection using OPDs by constructing active layers with PIN junction geometry based on the sequential layer-by-layer deposition of p-type polymers and [6,6]-phenyl C_{61} butyric acid methyl ester ($PC_{61}BM$). Because the front side of the incident light pathway is fully composed of pristine p-type polymers that cannot dissociate excitons into fre

e electrons and holes, only excitons generated from photons with low extinction coefficient can reach t he depletion region and can be dissociated as free hole and electron to contribute to external current. I n the previously reported CCN method, [8] all of the generated excitons are firstly dissociated, and a ver y thick active layer leads to the extraction of the selected holes and electrons exclusively. However, in the present work, PIN junction allows us to dissociate only specific excitons reaching the depletion re gion such that a considerably thinner active layer can be utilized. In addition, it was determined that t he pristine p- and n-layers at each charge-collecting interface of the PIN-OPD blocked the undesired in jection of dark current, leading to an ideal diode operation with an ideality factor of 1.3 and effective dark current injection barrier height of 0.69 eV. Thus, a high specific detectivity of 1.8×10^{12} Jones, linear dynamic range (LDR) of 91.3 dB, and -3 dB bandwidth of 15 kHz were demonstrated for the case study of red-selective OPDs. Finally, we demonstrated thin-film R/G/B full-color PIN-OPDs with detectivity over 1.0×10^{12} Jones.

II. Results & Discussion

The key idea of selective exciton activation is to realize full-color OPDs with significantly thinner active layer thickness compared to the case of Si-photodiode. The operation mecha-nism of previously reported CCN is based on different absorption behavior between photons

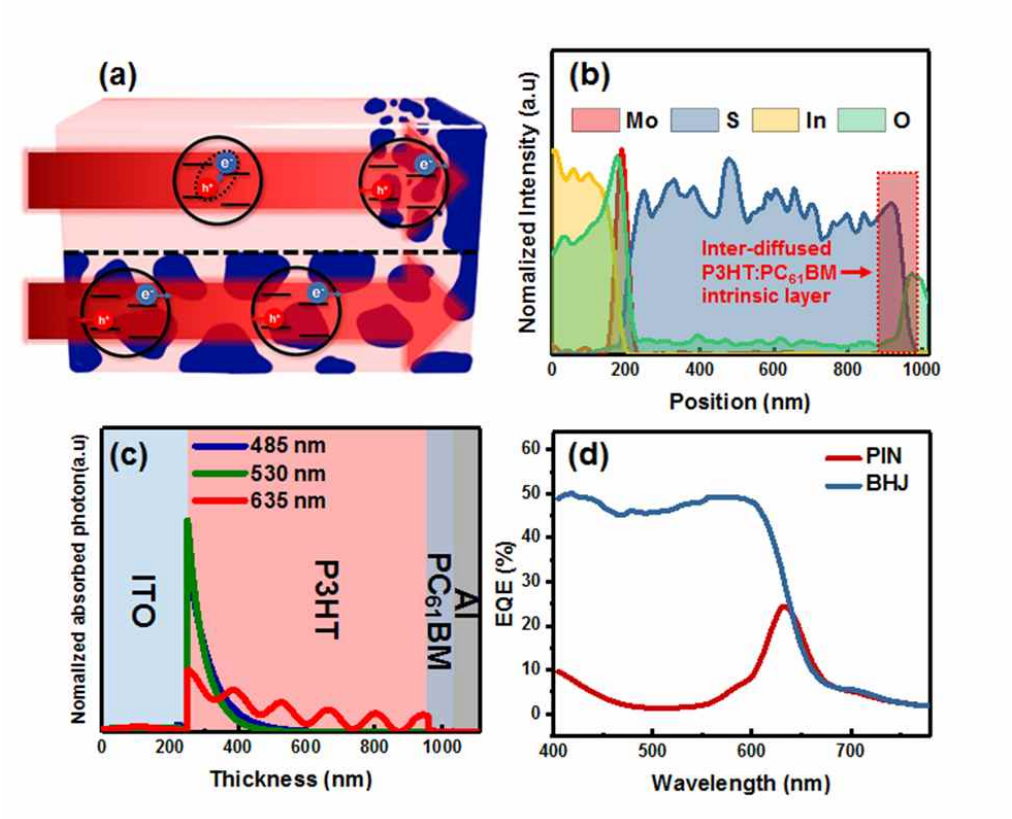

Figure 1. a) The schematic diagram describing (upper) the selective exciton activation mechanism in PIN-OPD in comparison to the case of (below) BHJ-OPD which separates all the generated excitons. b) EDS profiles of Mo, S, In and O element across the PIN-OPD. Each element corresponds to MoO_3, P3HT, ITO, and (partially) $PC_{61}BM$. c) The distribution profile of absorbed photons within PIN-OPD. d) The EQE spectra of PIN- and BHJ-OPDs.

with high and low absorption coefficients for the bulk heterojunction active layer. The incident photon with low extinction coefficient is absorbed across the entire active layer following cavity absorption behavior, while the incident photon with high extinction coefficient is fully absorbed at the front surface of the active layer following Beer-Lambert law. In this case, because all absorbed photons can generate free holes and electrons, the use of very thick active layer, with a thickness exceeding 1.5 μm, is essential to suppress the charge ex-

traction from the front surface of the active layer such that photons with high extinction coefficient can be ignored. In other words, as seen in Figure 1(a), due to the nature of BHJ, which provides a chance of exciton-dissociation everywhere within the active layer, some portion of photons with high extinction coefficient might contribute to photocurrent if the active layer is not sufficiently thick to suppress such surface-generated carriers. In a strong contrast, because PIN junction allows exciton-dissociation only at the narrow depletion region, the only photons arriving near the depletion region can contribute to photocurrent, and photons with high extinction coefficient mostly absorbed near the surface simply follow the monomolecular geminate recombination even when the active layer thickness becomes significantly thin. To confirm this hypothesis, both the BHJ and PIN-based OPDs were fabricated with relatively thin active layer of thickness ~800 nm, and their OPD performances were compared to one another. In both cases, we used poly(3-hexylthiophene-2,5-diyl) (P3HT) as an electron donor and $PC_{61}BM$ as an electron acceptor for constructing the active layer. For blend formulation of BHJ, 1:1 weight ratio was used and PIN-OPD was constructed by sequential deposition of P3HT and $PC_{61}BM$ with near-orthogonal solvents of chloroform and dichloromethane, respectively. Although the $PC_{61}BM$-dissolved dichloromethane solution did not seriously at-

tack the pre-deposited P3HT layer during spin-coating, [10] however the post-thermal treatment introduced inter-mixed phase between homogenous P3HT and $PC_{61}BM$ as seen in the cross-section transmission electron microscopy image of Figure 1(b). The thickness of each of P3HT and $PC_{61}BM$ was determined by transfer matrix optical simulation shown in Figure 1(c). The distribution profile of light absorption can be calculated using the formula

$$G = \frac{\varepsilon_0 \alpha(\lambda) n(\lambda) |E|^2}{2h} \quad (1)$$

where $|E|^2$ is the distribution of the optical field, $\alpha(\lambda)$ is the absorption coefficient of each layer, λ is the wavelength of the incident light, h is the Planck's constant, ε_0 is the vacuum permittivity, and n is the real part of the refractive index. [10] The structure used in the transfer-matrix optical simulation is ITO (200 nm) / molybdenum oxide (MoO_x) (30 nm) / P3HT (708 nm) / $PC_{61}BM$ (70 nm) / Al (100 nm). Optical simulation showed that the photons of green (530 nm) and blue (485 nm) wavelength were mostly absorbed in the pristine P3HT layer when the thickness of the P3HT layer was 708 nm and that the photons of red (635 nm) wavelength region can reach the interface of P3HT and $PC_{61}BM$. The experimentally obtained external quantum efficiency (EQE) spectra of BHJ- and PIN-OPDs with the similar

active layer of thicknesses ~800 nm are summarized in Figure 1(d). In the case of BHJ-OPD, the resulting EQE spectrum is similar to the absorption spectrum of P3HT:$PC_{61}BM$ blend film, implying that CCN mechanism is not realized due to the relatively low thickness (<< 1.5 μm). However, the PIN-OPD has a red-selective EQE spectrum with a peak at 635 nm, implying the realization of efficient selective exciton activation mechanism. Therefore, we can argue that PIN-OPDs are more beneficial to fully realize the color-selective photodiodes, especially with thinner active layer thickness. Despite the benefit of wavelength-selective detection of PIN-OPD, the overall EQE values were lower compared to BHJ-OPD, primarily because of the limited donor-acceptor interfacial area. However, as discussed in the following session, lower EQE values of PIN-OPD can be compensated by lower noise current, enabled by an ideal suppression of dark current injection.

The specific detectivity, D^*, the figure-of-merit of OPD is defined as:

$$D^* = \frac{q\lambda EQE\sqrt{A}}{hci_n} \quad (2)$$

where q is the elementary charge, λ is the illumination wavelength, A is the area of the active layer, c is the speed of light, and i_n is the noise current. [1,3] As can be seen from the above

equation, not only high *EQE* but also low i_n are important for high *D**. In most cases with optimized measurement set-up, the noise current is dominated by the shot noise current, which means that the value of *D** can be increased by reducing the dark current density. Here, we want to address that PIN-OPD can yield inherently low dark current compared to BHJ-OPD due to the morphological difference. In BHJ-OPDs, the P3HT and $PC_{61}BM$ domains are simultaneously exposed to both electrodes, thereby increasing the possibility of the unwanted hole and electron injection under reverse bias. However, in the case of PIN-OPDs, only $PC_{61}BM$ exists on the cathode surface and only P3HT exists on the anode surface, which can minimize unwanted hole and electron injection under reverse bias. Considering that dark current densities are determined by Boltzmann-type energetic uphill injection of hole/electron at each electrode under reverse bias, one can easily speculate that PIN-OPDs are significantly more advantageous than BHJ-OPDs.

In order to confirm the more efficient dark current suppression ability of PIN-OPDs, temperature dependent dark current density–voltage (J_d–V) relations were measured for both BHJ- and PIN-OPDs in the temperature range from 293 K to 173 K. The resulting J_d–V char-

acteristics were analyzed using a diode equation. Typically, the dark current density of an ideal diode is defined as

$$J_d = J_s \left[\exp\left(\frac{q(V - J_d R_s)}{\eta k T}\right) - 1\right] \quad (3)$$

where J_s is the dark saturation current density, V is the applied voltage, R_s is the series resistance, k is the Boltzmann's constant, T is the temperature, and η is the ideality factor. [11] Assuming that Boltzmann-type energetic uphill injection in OPD follows thermionic emission theory, which is widely accepted for Schottky barrier injection, the dark saturation current can be described by

$$J_s = A^* T^2 exp(\frac{-\varphi_B}{kT}) \quad (4)$$

where A^* is the Richardson constant, and φ_B is the effective barrier height. [12] Therefore, the slope of $\ln(J_s T^{-2})$ versus $(kT)^{-1}$ plot can provide φ_B. In Figure 2(a) and (b), J_d–V relations with various temperatures are shown for the PIN- and BHJ-OPDs, respectively, and in Figure 2(c), $\ln(J_s T^{-2})$ vs. $(k_B T)^{-1}$ plots are summarized. The obtained effective barrier height of PIN-OPD was found to be 0.69 eV, which is significantly higher than 0.25 eV of BHJ-OPD, supporting the abovementioned dark current suppressing effect of PIN-OPD. Assisted by the deeply

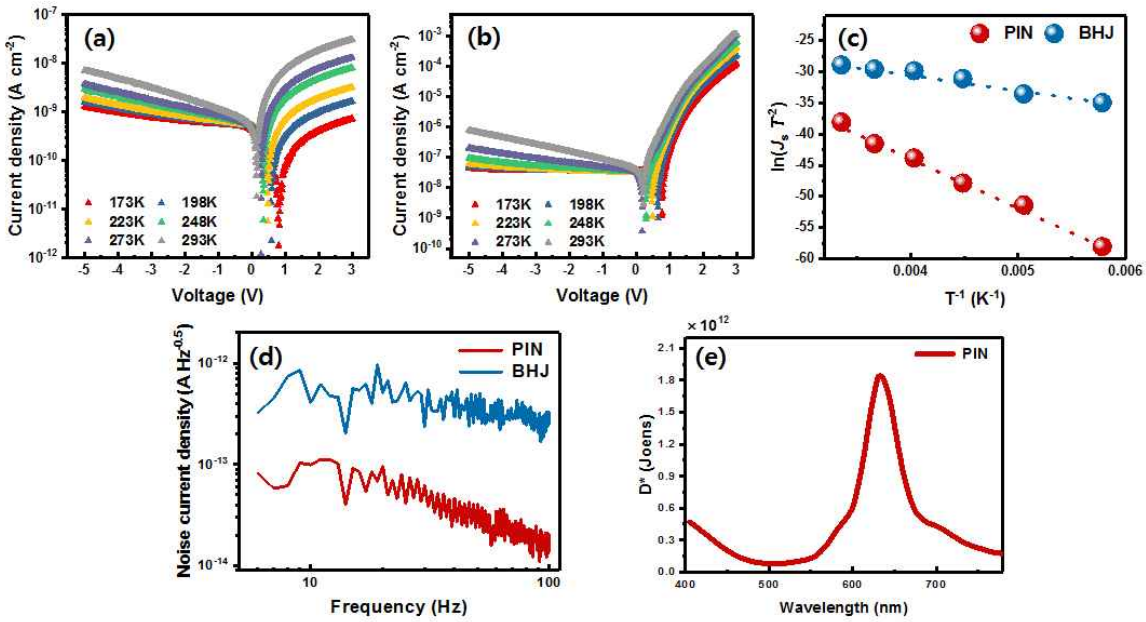

Figure 2. J_d–V characteristics of (a) PIN- and (b) BHJ-OPD measured at various temperature conditions, (c) ln(J_s T^{-2}) vs T^{-1} plot to calculate effective barrier height of PIN- and BHJ-OPD, (d) noise spectra for PIN- and BHJ-OPD and (e) specific detectivity spectrum of the optimized PIN-OPD.

suppressed dark current, low noise current density could be obtained for PIN-OPD as summarized in Figure 2(d), and thus high-detectivity red-selective OPD could be realized as shown in Figure 2(e).

Furthermore, to gain deep insight into the charge trap and recombination mechanism of PIN-OPD, we analyzed the ideality factor. In the absence of traps and recombination charges, the ideality factor has a value of unity. However, most photodiodes have values ranging between 1 and 2 due to non-ideality of the fabricated OPDs. [13] Figure 3(a) shows the relation-

ship between dV dJ_d^{-1}vs. J_d^{-1} for both BHJ- and PIN-OPDs. By rearranging Equation 3, we can fit the experimental data to obtain the ideality factor. (Supplementary Data) In the case of the PIN-OPD, the blocking roles of the pristine *p*- and *n*-layers at each electrode enabled the near-unity ideality factor of 1.3, which is significantly lower than 1.5 of BHJ-OPD.

For a variety of photodiode applications, a fast response and a wide dynamic range are essential. Since response rate lower than 100 Hz, especially in video applications, can give rise to a sense of discomfort in viewers, photodiodes with response rates above 100 Hz are recommended. We measured the -3 dB bandwidth (f_{3dB}), defined as the point at which the response signal power is -3 dB relative to the response signal power under continuous wave modulation. In Figure 3(b), the -3 dB point of the optimized PIN-OPD was determined as 15 kHz under reverse bias of 0.5 V, which is sufficiently fast for video applications.

In addition, for more accurate expression of brightness of image, it is important to have a constant responsivity for wide range of light intensities. This is expressed as linear dynamic range (LDR), which is defined as

$$\mathbf{LDR} = \mathbf{20}\ \mathbf{log}\left(\frac{J_{max}}{J_{min}}\right) \quad (5)$$

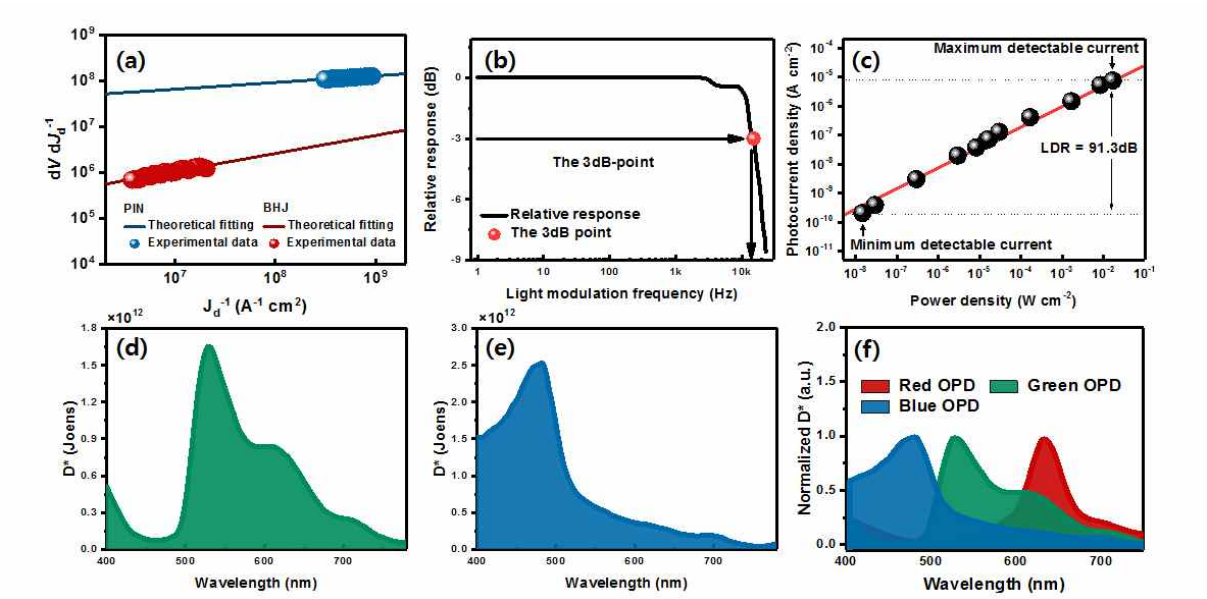

Figure 3. (a) dV dJ_d^{-1} vs J_d^{-1} plot to calculate ideality factor (dots and line correspond to experimental data and theoretical fitting, respectively), (b) the frequency response of PIN-OPD and (c) the dynamic response of PIN-OPD under reverse bias of 0.5 V and a 650 nm illumination with various light intensities. The -3 dB point and -3 dB frequency point are specified with the red dot and arrows. The measured specific detectivity spectra of the (d) green- and (e) blue-selective OPDs under reverse bias of 0.5 V and (f) a full-color photodetection spectrum using suggested OPDs.

where J_{max} and J_{min} are the maximum and minimum value of the measurable current density, respectively. [2,3] The measured LDR of the PIN-OPD under reverse bias of 0.5 V was 91.3 dB,(Figure 3(c)) which is comparable to the values of recently reported high performance OPDs. [14,15]

Finally, to realize R/G/B full-color OPDs, we further demonstrated green- and blue-selective thin film OPDs by using the PIN junction. In the case of green-selective OPD, we

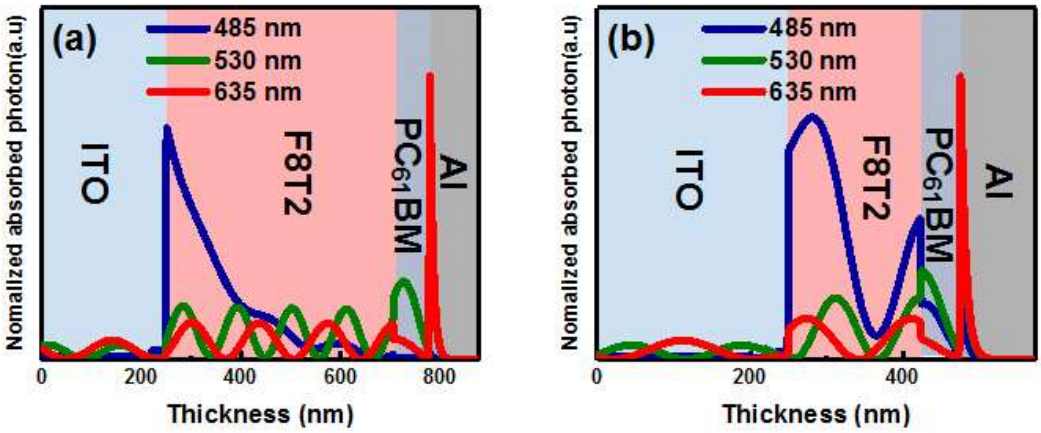

Figure 4. Simulated distribution profiles of absorbed photons of the suggested (a) green- and (b) blue-selective OPDs.

introduced F8T2 instead of P3HT as a *p*-type polymer, in order to shift the overall green selective exciton activation mechanism to shorter wavelength. F8T2 has blue-shifted absorption compared to P3HT by approximately 150 nm. Therefore, in this case, green photon with low extinction coefficient can be amplified in the final detectivity spectrum as shown in Figure 3(d) with a peak detectivity of 1.7×10^{12} Jones. In the case of blue-selective OPD, without the necessity of realizing selective exciton activation, we attempted to convert the original absorption range of F8T2 to the final detectivity spectrum entirely, because F8T2 has selectivity for blue wavelength range. Nonetheless, considering the overall ascendency of PIN-OPDs over BHJ-OPDs especially in terms of dark current suppression, we could realize blue-selective PIN-OPD with peak detectivity of 2.6×10^{12} Jones as seen in Figure 3(e). Optical

simulation results for green- and blue-OPDs are summarized in Figure 4. A full-color photo-detection spectrum using PIN-OPD is demonstrated in Figure 3(f). This is the first demonstration of thin film (total thickness below 1 μm) full-color OPDs, which can be an important technical advance for high-resolution image sensor.

III. Conclusion

In summary, we have demonstrated the filter-less set of red, green, and blue OPDs with a thin active layer film. To achieve the such full-color detection with a thin active layer, we introduced a selective exciton activation mechanism. Strategically designed PIN junction allowed only specific excitons to be separated while all other excitons were abandoned such that the final detectivity spectrum could be engineered even with a considerably thinner active layer. In addition, PIN junction with well-defined *p*- and *n*-layers at each electrode interface allowed the efficient suppression of the dark current under the reverse saturation regime with an effective barrier height of 0.69 eV and thus a low dark current density. As a result, in

this work, we could demonstrate a thin film (<1 μm) high detectivity (>10^{12} Jones) R/G/B full-color OPDs.

Experimental Section

Materials and Device Fabrication: Poly(3-hexylthiophene-2,5-diyl) (P3HT), Poly(9,9-dioctylfluorene-alt-bithiophene) (F8T2) were purchased from Sigma-Aldrich and [6,6]-phenyl C61 butyric acid methyl ester ($PC_{61}BM$) were purchased from Nano C. The materials were used without further purification.

Device fabrication: The organic photodiodes (OPDs) were fabricated on pre-patterned indium tin oxide (ITO) glass substrates (10 Ω sq^{-1}). The ITO-coated glass substrates were cleaned with a detergent, deionized water, acetone, isopropyl alcohol, and deionized water, by sequential ultrasonication for 20 mins each. The MoO_x films were deposited through a shadow mask with a thermal evaporator at the deposition rate of 0.2 Å s^{-1} and a vacuum pressure of ~10^{-6} Torr.

In the case of PIN-OPD, a P3HT solution of 40 mg mL^{-1} in chloroform was spin-casted onto the MoO_x-coated substrates at 500 rpm for 60 s, creating a layer with a thickness of ~700 nm. Then a $PC_{61}BM$ solution of 10 mg mL^{-1} in dichloromethane were spin casted at 1000 rpm onto the P3HT layer followed by thermal annealing at 100 ℃ for 10 min to create a PIN junction geometry. In the case of bulk heterojunction(BHJ)-OPD, a P3HT:$PC_{61}BM$ solution

of 60 mg mL^{-1} in chloroform was spin-casted onto the MoO_x-coated substrates at 1000 rpm for 60 s. Then, the BHJ film were annealed at 150 ℃ for 10 min. In the case of green- and blue-selective OPDs, a F8T2 solution of 20 mg mL^{-1} in chlorobenzene was spin-casted at 500 rpm for 60 s and a F8T2 solution of 10 mg mL^{-1} in chlorobenzene was spin-casted at 1000 rpm for 60 s onto the MoO_x-coated substrates, respectively. To complete the fabrication of OPDs, Al were deposited through a shadow mask with a thermal evaporator at the deposition rate of 0.5–1 Å s^{-1} and the vacuum condition about ~10^{-6} Torr.

J_d-V curve analysis: Equation 3 can be re-written as

$$\frac{dV}{dJ_d} = \frac{\eta kT}{q(J_d + J_S)} + R_s$$

(S1)

In the equation, ideality factor was obtained by using slope of the dV / dJ_d *vs.* J_d^{-1} plot.

Device characterization: The dark current density–voltage (J_d–V) characteristics were measured using a Keithley 4200 source measurement unit. The photocurrent spectra were measured using Keithley 2400 under monochromatic illumination from a 150-W Xenon arc lamp assembled with the Oriel Cornerstone 130 1/8 m monochromator. The noise measurement was conducted with a SR830 Lock-in Amplifier. For the measurement of the LDR, a mono-

chromator and a 650-nm laser (4.8×10^{-5} W cm^{-2}) were used. To measure the -3 dB frequency, the same laser was used with a TDS5052 digital phosphor oscilloscope (Tektronix) with a measured light intensity of 1 mW cm^{-2}.

Measurement: The cross-sectional transmission electron microscopy (TEM) image and energy dispersive spectroscopy profile of PIN-OPD was analyzed by high-resolution TEM (HF-3300. Hitachi). The thickness of films was measured by profilometer (DektakXT, BRUKER).

Optical simulation: *The optical electronic field and optical absorption simulation was performed by using the transfer matrix method. Optical constants were measured by using a V-VASE ellipsometer (Woollam Inc.).*

References

[1] Jansen-van Vuuren, R. D.; Johnstone, K. D.; Ratnasingam, S.; Barcena, H.; Deakin, P. C.; Pandey, A. K.; Burn, P. L.; Collins, S.; Samuel, I. D. W. Determining the Absorption Tolerance of Single Chromophore Photodiodes for Machine Vision. *Appl. Phys. Lett.*, 96, 2010, pp. 253303.

[2]. Jansen-van Vuuren, R. D.; Armin, A.; Pandey, A. K.; Burn, P. L.; Meredith, P. Organic Photodiodes: The Future of Full Color Detection and Image Sensing. *Adv. Mater.* 28, 2016, pp. 4766-4802.

[3] Baeg, K. J.; Binda, M.; Natali, D.; Caironi, M.; Noh, Y. Y. Organic Light Detectors: Photodiodes and Phototransistors. *Adv. Mater.* 25, 2013, pp. 4267-4295.

[4]. Knipp, D.; Herzog, P. G.; Stiebig, H. Stacked Amorphous Silicon Color Sensors. *IEEE Trans. Electron. Dev*, 49, 2002, pp. 170-176.

[5] Lee, K. H.; Leem, D. S.; Sul, S.; Park, K. B.; Lim, S. J.; Han, H.; Kim, K. S.; Jin, Y. W.; Lee, S.; Park, S. Y. A High Performance Green-Sensitive Organic Photodiode Comprising a Bulk Heterojunction of Dimethyl-Quinacridone and Dicyanovinyl Terthiophene. *J. Mater. Chem. C*, 1, 2013, pp. 2666-2671.

[6] Yoon, S.; Ha, J.; Cho, J.; Chung, D. S. Nonabsorbing Acceptor-Based Planar Heterojunction for Color-Selective and High-Detectivity Polymer Photodiodes. *Adv. Opt. Mater.* 4, 2016, pp. 1933-1938.

[7] Kim, K.; Sung, M. J.; Kwon, S. K.; Chung, D. S.; Kim, Y. H. Phenanthro [110, 9, 8-cdefg] Carbazole-Thiophene, Donor–Donor Copolymer for Narrow Band Green-Selective Organic Photodiode. *J. Phys. Chem. C.* 121, 2017, pp. 15931-15936.

[8] Armin, A.; Jansen-van Vuuren, R. D.; Kopidakis, N.; Burn, P. L.; Meredith, P. Narrowband Light Detection via Internal Quantum Efficiency Manipulation of Organic Photodiodes. *Nat. Comm.* 6, 2015, pp. 6343.

[9] Shen, L.; Fang, Y.; Wei, H.; Yuan, Y.; Huang, J. A Highly Sensitive Narrowband Nanocomposite Photodetector with Gain *Adv. Mater.* 28, 2016, pp. 2043–2048.

[10] Shafian, S.; Jang, Y.; Kim, K. Solution Processed Organic Photodetector Utilizing an Interdiffused Polymer/Fullerene Bilayer, *Opt. Express*, 23, 2015, pp. 936-946.

[11] Pettersson, L. A. A.; Roman, L. S.; Inganaˆs, O. J. Modeling Photocurrent Action Spectra of Photovoltaic Devices Based on Organic Thin Films. *Appl. Phys.* 86, 1999, pp. 487−496.

[12] Burkhard, G. F.; Hoke, E. T.; McGehee, M. D. Accounting for Interference, Scattering, and Electrode Absorption to Make Accurate Internal Quantum Efficiency Measurements in Organic and Other Thin Solar Cells *Adv. Mater.* 22, 2010, pp. 3293-3297.

[13] Troparevsky, M. C.; Sabau, A. S.; Lupini, A. R. Z.; Zhang, Y. Transfer-matrix formalism for the calculation of optical response in multilayer systems: from coherent to incoherent interference *Opt. Express.*, 18, 2010, pp. 24715-24721.

[14] Chen, S.; Zhang, G.; Liu, J.; Yao, H.; Zhang, J.; Ma, T.; Li, Z.; Yan, H. An All-Solution Processed Recombination Layer with Mild Post-Treatment Enabling Efficient Homo-Tandem Non-fullerene Organic Solar Cells *Adv. Mater.* 29, 2017, pp. 1604231

[15] Armin, A.; Hambsch, M.; Kim, I. K.; Burn, P. L.; Meredith, P.; Namdas, E. B. Thick junction broadband organic photodiodes *Laser Photonics Rev.* 8, 2014, 924–932.

[16] Armin, A.; Jansen-van Vuuren, R. D.; Kopidakis, N.; Burn, P. L.; Narrowband light detection via internal quantum efficiency manipulation of organic photodiodes Meredith, P. *Nat. Commun.* 6, 2015, pp. 6343.

[17] Lin, Q.; Armin, A.; Burn, P. L.; Meredith, P. Filterless narrowband visible photodetectors *Nat. Photonics* 9, 2015, pp. 687−694.

[18] Dou, L.; Yang, Y. M.; You, J.; Hong, Z.; Chang, W. H.; Li, G.; Yang, Y. Solution-Processed Hybrid Perovskite Photodetectors with high detectivity *Nat. Comm.* 5, 2014, pp. 5404.

[19] Qi, B.; Zhou, Q.; Wang, J. Exploring The Open-Circuit Voltage of Organic Solar Cells under Low Temperature. *Sci. Rep.* 5, 2015, pp. 11363.

[20] Street, R. A.; Schoendorf, M.; Roy, A.; Lee, J. H. Interface State Recombination in Organic Solar Cells. *Physical Review B*, 81, 2010, pp. 205307.

[21] Baierl, D.; Pancheri, L.; Schmidt, M.; Stoppa, D.; Dalla Betta, G. F.; Scarpa, G.; Lugli, P. A Hybrid CMOS-Imager with a Solution-Processable Polymer as Photoactive Layer. *Nat. Commun.* 3, 2012, pp. 1175.

[22] Guo, F.; Xiao, Z.; Huang, J.; Fullerene Photodetectors with a Linear Dynamic Range of 90 dB Enabled by a Cross-Linkable Buffer Layer, *Adv. Opt. Mater.* 1, 2013, pp. 289-

294.

Part 2. Surfactant-Induced Solubility Control to Realize Water-Processed High Precision Patterning of Polymeric Semiconductors for Full Color Organic Image Sensor

I. INTRODUCTION

Recently, the utilization of water as a processing solvent has been widely reported as an eco-friendly methodology for the treatment of polymer semiconductor devices. Although it is not easy to directly dissolve a polymer semiconductor having hydrophobic characteristics directly in water, it is well known that mini-emulsion synthesis using a surfactant enables good dispersion of various n-type, p-type and ambipolar conjugated polymers in water, resulting in the formation of water-borne colloids. Based on such water-borne colloid approaches, various electronic and opto-electronic applications have been demonstrated, including water-based organic field effect transistors (OFETs) and organic photovoltaics (OPVs).[1-6] However, these achievements were limited to single devices, and there has been no application of these water-borne colloids to complex devices such as eco-friendly displays, transistor backplane or image sensors, due to lack of methods for fine patterning these water-soluble polymers. Therefore, the development of a high-precision/throughput patterning technology for water-borne colloids to a similar technological level as polymer semiconductor patterning with organic solvents is very urgently required. Although ink-jet

printing can be a good solution, this process suffers from many reliability problems, especially with water-borne colloids. Due to the non-negligible size of polymer colloids (~100 nm), the size of the orifice may change during repeated injection, which can cause reliability issues in the shape and thickness of the pattern.[7-9] Because thin film deposition processes in water-borne colloids are more complex and demanding than those in organic solvents, particularly due to the multicomponent colloidal system including polymers, surfactants, and surfactant micelles, the corresponding patterning technique needs to be carefully designed, and must include a strategy to eliminate residual surfactants.[5]

Herein we introduce a surfactant-induced solubility control (SISC) method of water-borne polymeric colloids to realize environmentally-benign high-precision/throughput patterning of a full-color organic image sensor (OIS). In mini-emulsion synthesis, the hydrophobic tail groups of the surfactants are entangled with hydrophobic organic semiconductors, while the hydrophilic head groups directed to the water phase contribute to the dispersion, and thus the solubility, of the resulting colloidal polymer particles in water. Therefore, hydrophilic head groups dominate the surface properties of water-borne colloids, even after solidification processes such as spin-coating and dipping. Following the selective removal

of surfactant molecules from films of water-borne colloids, the films can recover their inherent hydrophobic surface nature of polymer semiconductors. In other words, the solubility of water-borne polymer semiconductors can be tuned dramatically from hydrophilic to hydrophobic, paving the way for fine patterning. Here we show systematic studies on the effects of various linear alcohols for the selective removal of surfactants. We demonstrate the efficient production by SISC of water-borne colloids, which enables high-precision/throughput patterning of multi-component polymer semiconductors. As a target application of the SISC method, the fabrication of a full-color, color filter-free and all-polymer water-processed image sensor array consisting of B-/G-/R-selective organic photodiode (OPD) pixels, each of 100 μm × 100 μm pixel size, is demonstrated. Furthermore, the image capture ability of the color filter-free 8 × 4 micro-pixel arrays is also demonstrated.

II. Results & Discussion

In the proposed SISC method, water is not only a dissolving solvent for polymer semicon-

ductors but also a pattern-developing solvent. The overall process sequence is graphically summarized in Scheme 1. The hydrophobic polymer (CYTOP) is spin-coated onto the pre-cleaned glass substrate with indium tin oxide (ITO) line-pattern with line width of 100 μm, followed by O_2-plasma treatment with a metal mask to form various hydrophilic wells. Then the prepared substrates are dipped into the first target water-borne colloidal solution. (In scheme 1, this is the red-selective poly([2,6′-4,8-

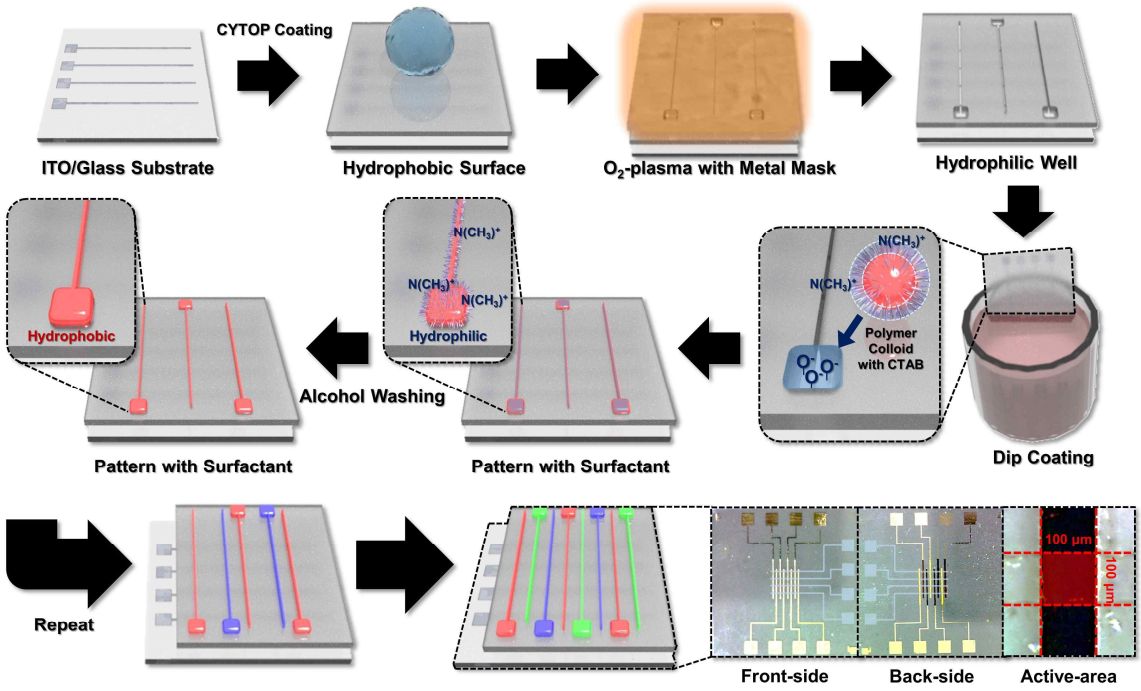

Scheme 1. Schematic description on SISC-based patterning method with B-/G-/R-selective water-borne colloid to fabricate color filter-free, full color OIS with the image of the suggested 8×4 patterned OIS and enlarged image of the active area of 100 μm × 100 μm size. Guide illustration of line-patterned ITO electrode with width of 100 μm is added for the reader's convenience.

di(5-ethylhexylthienyl)benzo[1,2-b;3,3-b]dithiophene]{3-fluoro-2[(2-ethylhexyl)carbonyl]thieno[3,4-b]thiophenediyl}) (PTB7-Th) colloids.) Note that here we adopted a Schottky junction architecture for each B-/G-/R-selective OPD, which can be operated without a color filter, and therefore, for each OPD, only one color-selective polymer semiconductor is used. The detailed operation mechanism of such a Schottky OPD can be found in the literature.[10-13] The thickness of the film was carefully adjusted by controlling the dipping speed. Then as a key step for realizing SISC, the substrate is dipped into alcohol, to selectively remove surfactants. The resultant surface of the patterned polymer film is hydrophobic and insoluble in water, because the

inherent hydrophobic nature of the polymer semiconductor was recovered by the successful removal of surfactant molecules. Therefore, the subsequent patterning process of the second target water-borne colloidal solution (in scheme 1, this is the blue-selective poly[[2,2′-bithiophene]-5,5′-diyl(9,9-dioctyl-9H-fluorene-2,7-diyl)] (F8T2) colloids), by repeating O_2-plasma treatment, dipping in water-borne colloidal solutions, and alcohol washing, does not affect the pre-patterned polymer layer. In this way, various polymer semiconductors with

totally different polarities or solubilities can be patterned with high precision/throughput. The actual device pattern image (8×4) was taken by optical microscope and inserted in Scheme 1 together with enlarged device active area image (100 μm × 100 μm). In addition, Bayer pattern which is typically used for commercial image sensor is also demonstrated in Figure 5(a), with a pattern size of 150 μm × 150 μm. To prepare a well-dispersed water-borne colloid solution for each B-/G-/R-selective polymer of F8T2/poly(3-hexylthiophene-2,5-diyl) (P3HT)/PTB7-Th, we employed cetrimonium bromide (CTAB) as a surfactant to minimize the quantity of surfactant used for these polymers in mini-emulsion synthesis, as clarified by an earlier study.[5] Figure 5(b) shows the dynamic light scattering (DLS) measurement results for water-borne colloids of F8T2/P3HT/PTB7-Th. All the employed polymers showed narrow size distribution with an average size of 60-70 nm. After dip-coating onto the patterned CYTOP substrate, as explained above, all the films were exposed to alcohol

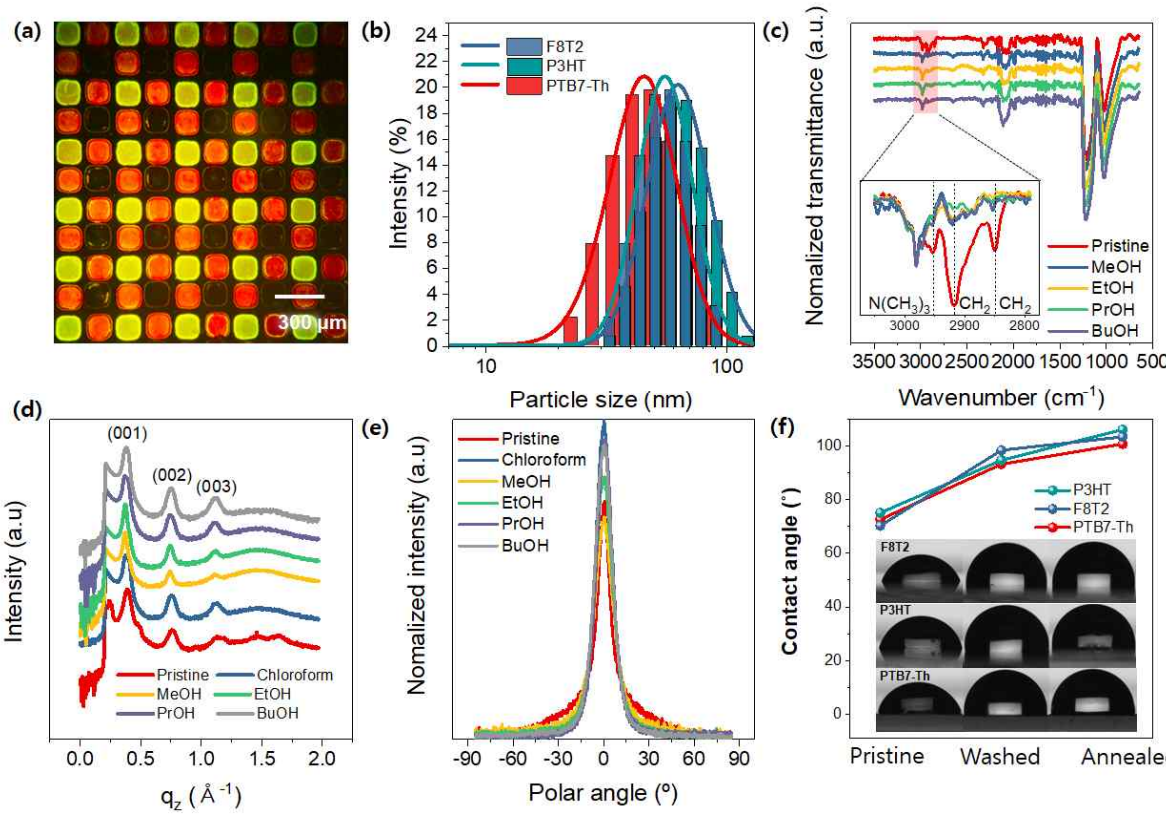

Figure 5. (a) Optical microscope image of B-/G-/R-selective polymer semiconductor patterns with pixel size of 150 μm × 150 μm under UV illumination (350 nm) and (b) size distribution of water-borne colloids of B-/G-/R-selective polymer semiconductor measured by DLS (c) FT-IR spectra of G-selective colloid-based films before and after post-treatment for washing with various linear alcohols. (d) Cross-sectional profile cut along the q_z axis (out-of-plane) of 2D GIXD patterns and (e) pole figure analyses for P3HT films cast from water-borne colloids with all the alcohol as the washing solvent and a film cast from chloroform. (f) Water contact angle on B-/G-/R-selective colloids film, in the sequence of pristine, washed with PrOH and post-annealing. The inset is the photograph of the water contact angle image.for surfactant removal and to realize the SISC method. Before conducting experiments for surfactant removal, the solubility parameters of CTAB, polymer semiconductors and alcohols were comparatively studied. The dispersion, polar, and hydrogen parameters were calculated by the group contribution method, and each parameter.

is summarized in Table S1.[14, 15] As the alkyl chain length of the alcohol increases, the polar

and hydrogen bonding parameters decrease, while the dispersion parameter increases. The total solubility parameter of n-propanol (PrOH) with 23.6 $MPa^{0.5}$ is most similar to the total solubility parameter of CTAB with 24.9 $MPa^{0.5}$. For this reason, CTAB removal efficiency - which involves the weakening of the original van der Waals force between the polymer and CTAB, and the formation of a new van der Waals force between CTAB and PrOH - was expected to be the highest in films washed with PrOH. Figure 5(c) shows Fourier-transform infrared (FT-IR) analyses results of G-selective colloid to compare the surfactant removal efficiency of water-borne colloids washed with methanol (MeOH), ethanol (EtOH), PrOH, and n-butanol (BuOH). In all the FT-IR spectra, features within the 2800 to 3000 cm^{-1} range, corresponding to vibration peaks originated from CTAB were dramatically reduced to negligibly small values as a result of alcohol washing (inset of Figure 5(c)), implying that the surfactants were selectively transferred to the alcohol phase, and this tendency was maximized with PrOH.[16, 17] Although these results support the hypothesis that the surfactant was successfully removed, it is not yet clear how the alcohol washing process affects the film cast from water-borne colloids. To investigate how alcohol affects the morphology of polymer semiconductor, grazing incidence X-ray diffraction (GIXD) analyses

were conducted for P3HT films cast from water-borne colloids with all the alcohols as the washing solvent and a film cast from chloroform (Figure 5(d)). Interestingly, in the case of the films cast from water-borne colloids followed by alcohol washing, well-developed lamellar stacking features of P3HT were observed, similar to the case of chloroform-deposited film. In order to get more quantitative information of the crystalline orientation of the films, we conducted pole figure analyses, as presented in Figure 5(e). For the pole figure analyses, we analyzed the distribution of the (002) orientations of five films to avoid the reflected beam. It is clearly seen that not only the chloroform-deposited film, but also all other colloid-based films have a preferential edge-on orientation. Interestingly, more oriented edge-on orientation is observed in the sequence of MeOH, EtOH, PrOH, which can be ascribed to more efficient washing of CTAB. However, in the case of the film washed with BuOH, possibly due to the too high dispersion solubility parameter of BuOH even similar to dispersion solubility parameter of P3HT, a slightly worse orientation was observed. Based on these observations, we proceeded with the patterning experiments using PrOH as a washing solvent. To further confirm the effectiveness of the SISC mechanism, surface energy analyses of the films cast from water-borne colloids of three different polymers

were conducted and the obtained water contact angles are summarized in Figure 5 (f), in the sequence of pristine, washed with PrOH and post-annealing. As expected, pristine films cast from water-borne colloids possess a hydrophilic surface due to surfactants with a ~70˚ water contact angle, while the hydrophobic nature is mostly recovered after washing with PrOH, followed by post thermal annealing. The surface energy values calculated from contact angle measurements with both water and diiodomethane are summarized in Table S2, showing efficient recovery of the hydrophobic nature of polymer semiconductors after PrOH washing. Thanks to the hydrophobic nature of polymer semiconductor pattern after PrOH washing, the surface morphology of the patterns was not damaged during sequential coating-then-washing processes with B-/G-/R-selective colloidal solution. In all the cases, the obtained FET mobilities were comparable to those obtained from organic solvent-based fabrication, indicating the feasibility of the suggested method. Collectively, these results show that

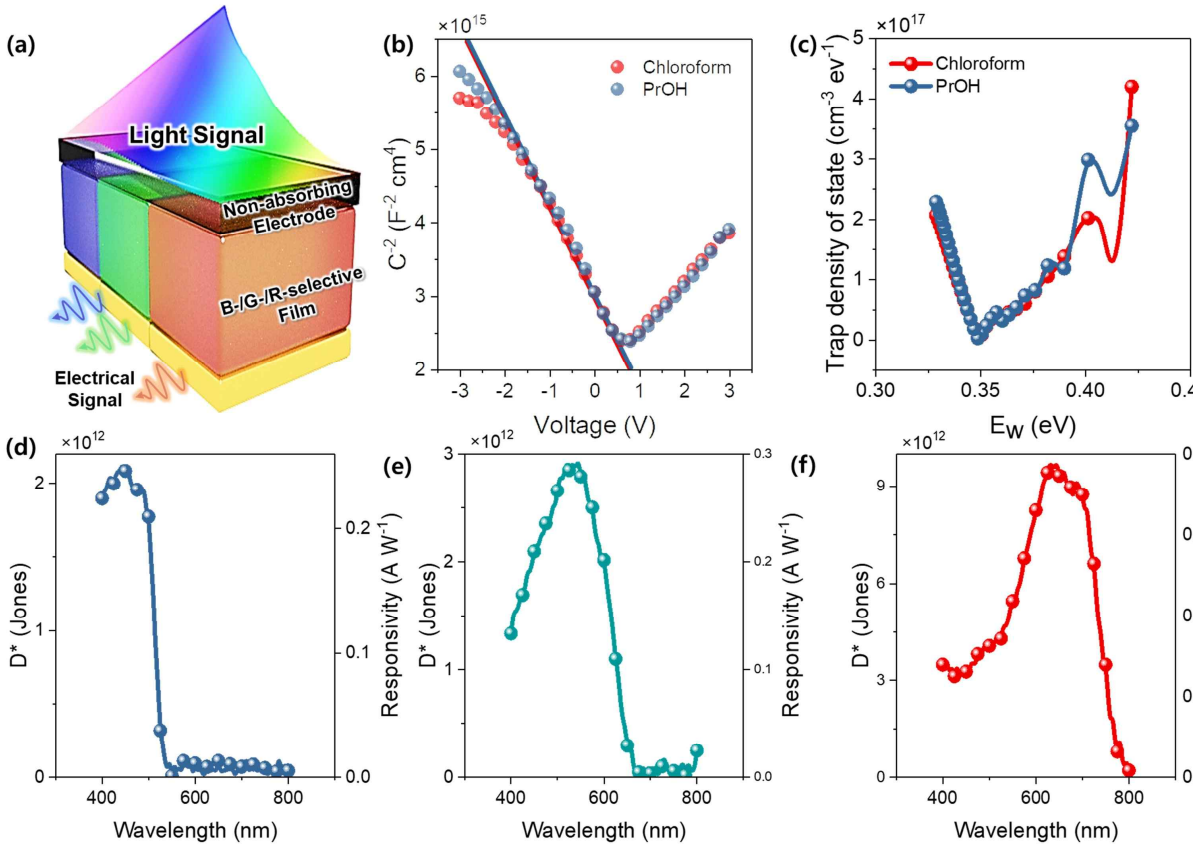

Figure 6. (a) Schematic description on the suggested OPD structured as ITO/ZnO (non-absorbing electrode)/B-/G-/R-selective film/Au. (b) Mott–Schottky plot of the suggested Schottky OPD with P3HT as an active layer for both water-borne colloids- and chloroform-devices to compare effective V_{bi} and N_d. V_{bi} and N_d are determined from the intercept with x-axis and slope of onset, respectively. (c) Estimated trap density of states measured by TAS. (d-f) Specific detectivity and responsivity spectra as a function of wavelength for B-/G-/R-selective OPDs.

the SISC method can endow high throughput/precision patterning of various polymers on the same substrate without the loss of inherent semiconducting properties, with water as the only processing solvent. As a target application of the SISC method, we demonstrate a col-or filter-free, high-performance full color OIS. Unlike other electronic and optoelectronic

applications, image sensors require B-/G-/R-patterns with three different compositions and are therefore an optimal platform to show the full advantage of the SISC method. For this application, we introduced a Schottky organic photodiode (OPD) architecture (Figure. 2 (a)) to construct each unit pixel, where a single semiconductor component is used in junction with a transparent metal electrode to construct a Schottky junction. In this case, because a single semiconductor component is responsible for light absorption, finely controlled color reproduction is possible from the resulting OPD by a carefully designed absorption feature of the semiconductor.[12] Therefore, a key to the success of the water-processed color filter-free, full-color image sensor relies on the quality of the generated Schottky junction properties between the ITO/ZnO electrode and the SISC-patterned polymer layer. In order to characterize the fabricated Schottky junction, Mott–Schottky analyses were conducted for the Schottky diode structured as ITO/ZnO/P3HT (water-borne colloids- and chloroform-based film)/MoO_3/Au in comparison to the organic solvent-fabricated equivalents and the resulting plots are shown in Figure 2 (b). The intercept to the x axis of the tangent to the onset can be interpreted as the built-in potential (V_{bi}) of the diode, and it shows a similar value of ~ 0.85 eV, in both the SISC and organic solvent systems. The do-

nor concentration (N_d) can also be extracted from the slope: 2.95 × 10^{16} cm^3 for the photodiode fabricated with organic solvent and 2.81 × 10^{16} cm^3 for the photodiode fabricated with SISC.[13] In addition, we conducted thermal admittance spectroscopy (TAS) to quantitatively study the deep trap states of the fabricated Schottky diode using the equation $N_T(E_v) = -\frac{V_{bi}}{qW}\frac{dC}{dv}\frac{v}{k_B T}$, where V_{bi} is the built-in potential, q is the elementary charge, W is the depletion width, C is the capacitance, v is the frequency, k_B is the Boltzmann constant, T is the device temperature, and E_v is defined as $E_v = k_B T ln\left(\frac{v_0}{v}\right)$, where v_0 is the attempt-to-escape frequency commonly considered as 10^{12} Hz. The value of W of the Schottky diode under open circuit conditions can be obtained by $W = \sqrt{\frac{2\varepsilon V_{bi}}{q N_d}}$.[13, 18, 19] Figure 2 (c) shows that the mid-gap state density spans a similar spectral range for both the SISC and organic solvent systems. Collectively, these junction analyses clearly show that the successful removal of residual surfactants and the recovery of the crystalline orientation of each B-/G-/R-selective polymer semiconductor enabled near-ideal junction formation even with the SISC patterning process. Here, specific detectivity (D^*), the figure-of-merit of OPDs, can be calculated by[20, 21]

$$D^* = \frac{R\sqrt{A}}{i_n} \quad (1)$$

where R is the responsivity, A is the area of the active layer, and i_n is the noise current. As can be seen from the above equation, not only high responsivity but also low i_n are essential for high D^*. The measured responsivity and D^* spectra are summarized in Figure 2. (d-f). Considering that a smaller photodiode pixel size often introduces a high surface leakage current, the fairly high level of D^* (over 10^{12} Jones) observed for all the patterned (100 μm × 100 μm) B-/G-/R-selective OPDs clearly demonstrates the effectiveness of the SISC method, especially for precise patterning.[22, 23] For accurate image extraction, not only high D^* but also narrow distributions of responsivity among all the patterned pixels are essential.[24] The responsivity of B-/G-/R-selective photodiodes were measured from each pixel of the 8×4 pixel array, as summarized in Figure 7 (a), (b) and (c). Average responsivity of 0.24, 0.30 and 0.32 A W^{-1} with standard deviations of 0.049, 0.060 and 0.049 A W^{-1} were obtained for the B-/G-/R-selective photodiodes, respectively. The detectable light intensity range and

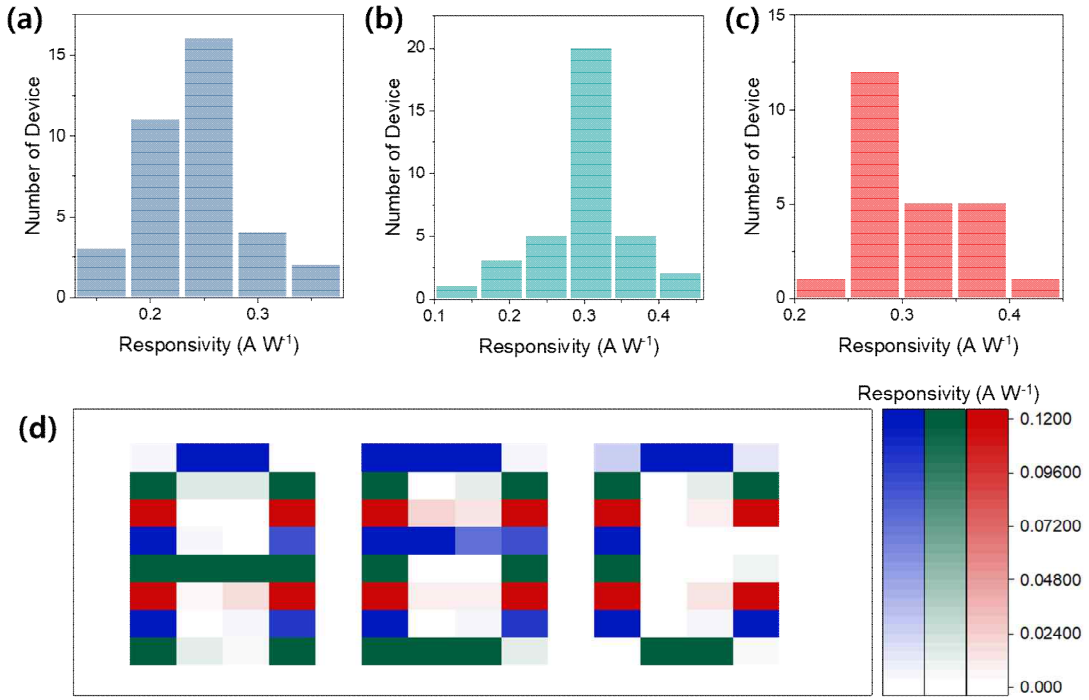

Figure 7. Responsivity distributions of the (a) B-/ (b) G-/ (c) R-selective OIS pixels. The statistical responsivities were 0.24 ± 0.049, 0.30 ± 0.060 and 0.32 ± 0.049 A W^{-1} for B-/G-/R-selective OIS pixels, respectively. (d) Graphically reconstructed ABC image captured from OIS based on responsivities of each constituting B-/G-/R-selective OPDs when blue (450 nm, 43.1 μW cm^{-2}), green (550 nm, 33.6 μW cm^{-2}) and red (650 nm, 31.7 μW cm^{-2}) photons were illuminated through A-, B-, and C-shaped shadow mask.

operating speed of the OPD can be represented by the linear dynamic range (LDR) and 3-dB bandwidth (f_{3dB}). These two parameters of OPDs are important for a wider application range of the image sensor. f_{3dB} is defined as the point at which the response signal power is 3-dB relative to the response signal power under continuous wave modulation. [20, 25-27] LDR is calculated by:[20, 25-28]

$$LDR = 20\log\frac{I_{min}}{I_{max}} \quad (2)$$

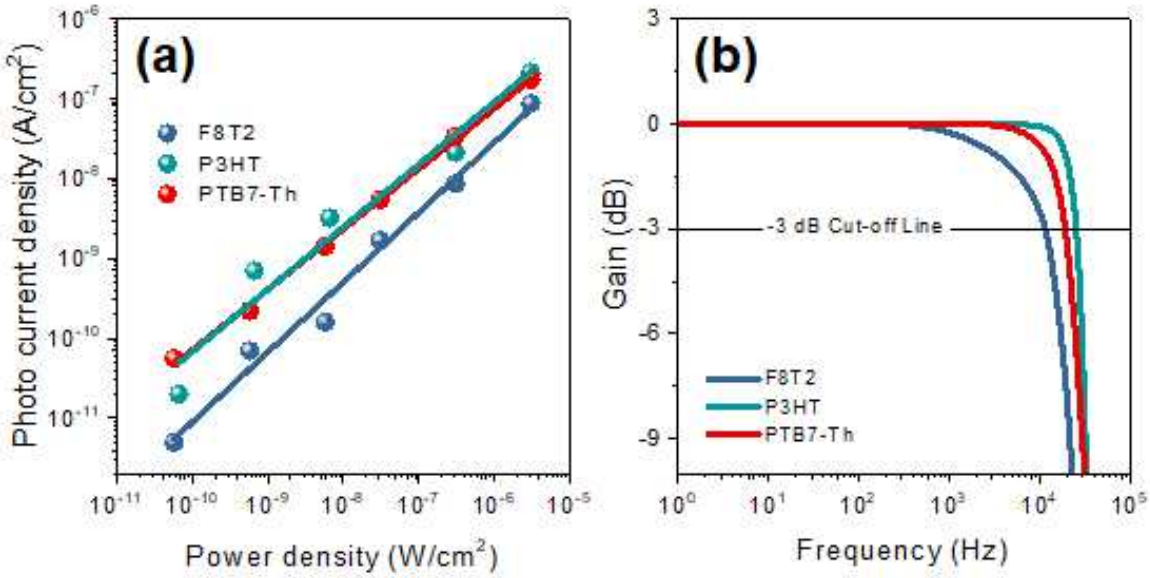

Figure 8. (a) −3 dB cutoff frequency and (b) LDR of OPDs of the suggested B-/G-/R-selective photodiode with F8T2/P3HT/PTB7 colloids.

where I_{max} and I_{min} are the maximum and minimum values of the measurable current, respectively. f_{3dB} of the optimized B-/G-/R-selective OPDs were determined > 20 kHz, and the LDR of the optimized B-/G-/R-selective OPDs were determined > 75 dB at -0.01 V in Figure 8. To further simulate the imaging application of OISs, we investigated the image-capturing capability with differently-colored light sources as well as A, B, C-shaped patterned masks. As shown in Figure. 3 (d), the color filter-free OIS pixel arrays were constructed as line-by-line combination of B-/G-/R-selective OPDs; the B-selective OPDs are located at 1, 4 and 7 low, the G-selective OPDs are located at 2, 5 and 8 low, and the R-selective OPDs are located at 3 and 6 low. Four different light sources of red (650 nm),

green (550 nm), and blue (450 nm) were illuminated to the prepared OIS via A, B, C-shaped shadow masks, and the corresponding responsivity information from 32 pixels were collected using a home-built jig and software, followed by reconstruction of the R/G/B color intensity according to the measured responsivity. As clearly shown in Figure. 3 (d), we could capture the A, B, C-shaped images thanks to the uniform dark current and responsivity of the fabricated SISC-based color filter-free, full color OIS.

III. Conclusion

Polymer semiconductors are promising class of materials, which combine many of the electrical properties of inorganic semiconductors with the mechanical flexibility and chemical processability of organic materials. However, these polymer semiconductors are generally mutually soluble with other organics, thus preventing the drawbacks of solution-based deposition of complex patterned structures using standard photolithographic techniques. In this work, we developed a new polymer patterning method, SISC, where a surfactant is the key element for tuning the surface energy of films cast from water-borne colloids. Selective

removal of surfactant molecules from hydrophilic water-borne polymer colloids, which is enabled by PrOH in this work, can lead to the recovery of the hydrophobic nature of polymer semiconductors, and paves the way for high-precision patterning of polymer semiconductors with water as a processing solvent. As a target application of the suggested SISC-based polymer patterning, a full-color OIS was chosen because this requires lateral patterning of three different polymer components. The resulting patterned B-/G-/R-selective photodiodes, with a pixel size of 100 μm × 100 μm, show narrow-band absorption spectra with detectivity over 10^{12} Jones, enabling color filter-free OIS application. Thanks to the low pixel-to-pixel deviation of the fabricated OIS consisting of 8 × 4 pixels of polymer OPDs, its actual image capturing ability could be successfully demonstrated.

Experimental Section

Materials

MeOH, EtOH, PrOH, BuOH, chloroform, zinc acetate dihydrate, 2-methoxyethanol, ethanolamine and CTAB were purchased from Sigma-Aldrich. PTB7-Th and F8T2 were purchased from 1-Materials. P3HT was purchased from Rieke. CYTOP was purchased from AGC Chemicals. Purchased materials were used

without further purification steps.

Water-borne colloids Preparation

The B-/G-/R-selective polymer semiconductors of 30 mg were dissolved in chloroform of 10 ml. 100 mg of CTAB was dissolved in deionized water of 30 ml and added to a solution of B-/G-/R-selective polymer semiconductors. The solution was stirred for 5 min and sonicated for 1 min with a Branson Model 8510 Ultrasonic Cleaner. This procedure was repeated until the color of the solution no longer changed. Finally, chloroform was fully evaporated at 65 °C. To remove excess surfactant, the B-/G-/R-selective colloids solutions were dialyzed with Standard RC Tubing (MWCO: 12-14 kD), overnight.

OPD Fabrication

For fabrication of color-selective OPDs, glass substrates with 100 μm sized ITO line-pat-

tern were cleaned sequentially with detergent, deionized water, acetone and isopropanol by sonication and dried with nitrogen. Sol-gel based ZnO solution was prepared by adding 1 g of zinc acetate dihydrate and 0.28 g of ethanolamine in 2-methoxyethanol and stirred at 600 rpm for 6 hr. The sol-gel based ZnO solution was spin-coated onto the cleaned ITO substrate. Then CYTOP solution diluted by 1:3 vol% to the given solvent was spin-coated at 1000 rpm to render film thickness of 100 nm. CYTOP laye

r was patterned by O_2-plasma etching with metal mask aligned with home-built aligner and optical m icroscope (UM12 Microscope, Vitiny). After O_2-plasma treatment with metal mask, the B-/G-/R-selecti ve layers were fabricated by dip-coating. Excess ligands were removed by dipping in alcohol. Then, MoO_3 and Au were deposited through a shadow mask with 100 μm line-pattern using a thermal evapo rator at the deposition rate of 0.5 Å s^{-1} and the vacuum pressure of ~10^{-6} Torr. T he active layer of OPDs is defined as area between 100 μm sized ITO electrode and 100 μm sized gold electro de.

OFET Fabrication

The active layer was deposited by spin-coating on an OTS-treated SiO_2/Si substrate with Au S/D pat- tern. The resultant film was dipped in PrOH for 5 min and annealed at 200°C for 10 min. The channel W/L ratio was 12 with a channel width of 600 μm, and a channel length of 50 μm.

Device Characterization

UV-Vis-NIR absorption spectra of B-/G-/R-selective colloids films were measured using a U V-Vis-NIR absorption spectrophotometer (Cary 5000 UV-Vis-NIR, Agilent). The image of B-/G-/R-sele ctive colloids of the optimized photodiode was analyzed by high-resolution TEM (HF-3300, Hitachi). AFM images of P3HT pattern as a fucntion of the times of the coating-then-washing process were a

cquired by using AFM (Park Systems, XE-150). FT-IR absorbance peaks were acquired using an FT-IR spectrometer (FT/IR 4700, JASCO). The GIXD measurements were performed using the PLS-II 3C and 9A U-SAXS beamlines at the Pohang Accelerator Laboratory (PAL) in Korea. The transfer curve of organic field effect transistors (OTFTs) were measured using Keithley 4200A-SCS. Dark currents and responsivities of photodiodes were measured with Keithley 2400 sourcemeter and monochromatic light from 150 W Xe arc lamp. To measure linear dynamic range and 3-dB frequency, R/G/B lasers (650, 550, 450 nm) were additionally used with a TDS5052 digital phosphor oscilloscope (Tektronix). Noise current was directly measured from SR830 Lock-in amplifier with home-built LabView program.

References

[1] Kim, Y. J.; Lee, B., Unique p–n Heterostructured Water-Borne Nanoparticles Exhibiting Impressive Charge-Separation Ability. *ChemSusChem*, 11, 2018, pp. 1628-1638.

[2] Xie, C.; Classen, A.; Späth, A.; Tang, X.; Min, J.; Meyer, M.; Zhang, C.; Li, N.; Osvet, A.; Fink, R. H., Overcoming microstructural limitations in water processed organic solar cells by engineering customized nanoparticulate inks. *Advanced Energy Materials.* 8, 2018, pp. 1702857.

[3] Yu, S. H.; Song, H. G.; Cho, J.; Kwon, S.-K.; Kim, Y.-H.; Chung, D. S., Synthetic Approach for Enhancing Semiconductor Properties of Water-Borne DPP-Copolymer. *Chemistry of Materials*, 30, 2018, pp. 4808-4815.

[4] Cho, J.; Yu, S. H.; Chung, D. S., Environmentally benign fabrication processes for high-performance polymeric semiconductors. *Journal of Materials Chemistry C*, 5, 2017, pp. 2745-2757.

[5] Cho, J.; Yoon, S.; Sim, K. M.; Jeong, Y. J.; Park, C. E.; Kwon, S.-K.; Kim, Y.-H.; Chung, D. S., Universal selection rule for surfactants used in miniemulsion processes for eco-friendly and high performance polymer semiconductors. *Energy & Environmental Science*, 10, 2017, pp. 2324-2333.

[6] Zappia, S.; Scavia, G.; Ferretti, A. M.; Giovanella, U.; Vohra, V.; Destri, S., Water-Processable Amphiphilic Low Band Gap Block Copolymer: Fullerene Blend Nanoparticles as Alternative Sustainable Approach for Organic Solar Cells. *Advanced Sustainable Systems*, 2, 2018, pp. 1700155.

[7] Ando, B.; Baglio, S., All-inkjet printed strain sensors. *IEEE Sensors Journal*, 13, 2013, pp. 4874-4879.

[8] Sowade, E.; Ramon, E.; Mitra, K. Y.; Martínez-Domingo, C.; Pedró, M.; Pallarès, J.; Loffredo, F.; Villani, F.; Gomes, H. L.; Terés, L., All-inkjet-printed thin-film transistors: manufacturing process reliability by root cause analysis. *Scientific reports*, 6, 2016, 33490.

[9] Verkouteren, R. M.; Verkouteren, J. R., Inkjet metrology II: resolved effects of ejection frequency, fluidic pressure, and droplet number on reproducible drop-on-demand

dispensing. *Langmuir*, 27, 2011, 9644-9653.

[10] Sung, M. J.; Kim, K.; Kwon, S.-K.; Kim, Y.-H.; Chung, D. S., Phenanthro [110, 9, 8-cdefg] carbazole-thiophene, donor–donor copolymer for narrow band green-selective organic photodiode. *The Journal of Physical Chemistry C*, 121, 2017, pp. 15931-15936.

[11] Sung, M. J.; Yoon, S.; Kwon, S.-K.; Kim, Y.-H.; Chung, D. S., Synthesis of Phenanthro [1, 10, 9, 8-cdefg] carbazole-Based Conjugated Polymers for Green-Selective Organic Photodiodes. *ACS applied materials & interfaces*, 8, 2016, pp. 31172-31178.

[12] Yoon, S.; Ha, J.; Cho, J.; Chung, D. S., Nonabsorbing Acceptor-Based Planar Heterojunction for Color-Selective and High-Detectivity Polymer Photodiodes. *Advanced Optical Materials*, 4, 2016, pp. 1933-1938.

[13] Kim, K.; Sim, K. M.; Yoon, S.; Jang, M. S.; Chung, D. S., Defect Restoration of Low-Temperature Sol-Gel-Derived ZnO via Sulfur Doping for Advancing Polymeric Schottky Photodiodes. *Advanced Functional Materials*, 28, 2018, pp. 1802582.

[14] Hansen, C. M., Hansen solubility parameters: a user's handbook. CRC press: 2002.

[15] Van Krevelen, D. W.; Te Nijenhuis, K., Properties of polymers: their correlation with chemical structure; their numerical estimation and prediction from additive group contributions. *Elsevier*: 2009.

[16] Borodko, Y.; Jones, L.; Lee, H.; Frei, H.; Somorjai, G., Spectroscopic study of tetradecyltrimethylammonium bromide Pt— C14TAB nanoparticles: Structure and stability. *Langmuir*, 25, 2009, pp. 6665-6671.

[17] Truong, P. L.; Cao, C.; Park, S.; Kim, M.; Sim, S. J., A new method for non-labeling attomolar detection of diseases based on an individual gold nanorod immunosensor. *Lab on a Chip*, 11, 2011, pp. 2591-2597.

[18] Street, R. A.; Yang, Y.; Thompson, B. C.; McCulloch, I., Capacitance spectroscopy of light induced trap states in organic solar cells. *The Journal of Physical Chemistry C*, 120, 2016, 22169-22178.

[19] Shuttle, C. G.; Treat, N. D.; Douglas, J. D.; Fréchet, J. M.; Chabinyc, M. L., Deep energetic trap states in organic photovoltaic devices. *Advanced Energy Materials*, 2, 2012, pp. 111-119.

[20] Jansen-van Vuuren, R. D.; Armin, A.; Pandey, A. K.; Burn, P. L.; Meredith, P., Organic photodiodes: the future of full color detection and image sensing. *Advanced Mate-*

rials, 28, 2016, pp. 4766-4802.

[21] Sim, K. M.; Swarnkar, A.; Nag, A.; Chung, D. S., Phase Stabilized α-CsPbI3 Perovskite Nanocrystals for Photodiode Applications. *Laser & Photonics Reviews*, 12, 2018, pp. 1700209.

[22] Weisfield, R. L. In Amorphous silicon TFT X-ray image sensors, International Electron Devices Meeting 1998. Technical Digest (Cat. No. 98CH36217), *IEEE*: 1998, pp 21-24.

[23] Xue, Y.; Wang, Z.; Chen, W.; Liu, M.; He, B.; Yao, Z.; Sheng, J.; Ma, W.; Dong, G.; Jin, J., Proton Radiation Effects on Dark Signal Distribution of PPD CMOS Image Sensors: Both TID and DDD Effects. *Sensors*, 17, 2017, pp. 2781.

[24] Yang, B.; Pan, W.; Wu, H.; Niu, G.; Yuan, J.-H.; Xue, K.-H.; Yin, L.; Du, X.; Miao, X.-S.; Yang, X., Heteroepitaxial passivation of $Cs_2AgBiBr_6$ wafers with suppressed ionic migration for X-ray imaging. *Nature communications*, 10, 2019, pp. 1989.

[25] Armin, A.; Jansen-van Vuuren, R. D.; Kopidakis, N.; Burn, P. L.; Meredith, P., Narrowband light detection via internal quantum efficiency manipulation of organic photodiodes. *Nature communications*, 6, 2015, pp. 6343.

[26] de Arquer, F. P. G.; Armin, A.; Meredith, P.; Sargent, E. H., Solution-processed semiconductors for next-generation photodetectors. *Nature Reviews Materials*, 2, 2017, pp. 16100.

[27] Fang, Y.; Armin, A.; Meredith, P.; Huang, J., Accurate characterization of next-generation thin-film photodetectors. *Nat. Photonics*, 13, 2019, pp. 1-4.

[28] Armin, A.; Hambsch, M.; Kim, I. K.; Burn, P. L.; Meredith, P.; Namdas, E. B., Thick junction broadband organic photodiodes. *Laser & Photonics Reviews,* 8, 2014, pp. 924-932.

요 약 문

풀 컬러 이미징을 위한 고성능 유기 포토 다이오드 어레이의 제조 공정 개발

본 논문은 기존 무기물 기반 이미지센서가 가지는 색선택성, 높은 공정비용, 두꺼운 두께등의 문제를 해결하기 위해서 색 선택성 유기 반도체를 사용하여 유기 포토 다이오드 어레이를 제조하는 방법에 대한 논문입니다.
우선 유기반도체를 사용한 색 선택성 방법의 경우 두가지를 제시하였습니다. 첫번째는 선택성 여기자 추출 방법으로 두께에 따라 흡광이 달라지는 유기반도체의 특성을 이용하여 선택적으로 흡광을 조절하는 방법입니다. 각 P 형과 N 형 반도체의 두께를 선택적으로 조절하고 여기자를 추출하는 위치를 조절하여 색 선택성을 구현하였고 이를 통해 적색광, 녹색광, 청색광 광다이오드를 구현하였습니다. 두번째는 유기 반도체가 가지는 흡광을 이용하는 방법으로 유기반도체의 에너지 밴드 조절을 통해서 특정 영역의 빛을 흡수하는 유기반도체를 합성을 하고 이를 이용하여 선택적인 흡광을 얻을 수 있었습니다.
또한 공정 비용을 줄이고 대면적 박막형성이 가능한 용액공정을 이용하여 패턴을 형성하기 위해서 계면활성제를 이용한 용해도 변환 공정을 제시하였습니다. 기존 용액공정을 통해서 두개 이상의 패턴을 형성할 경우 기 형성된 패턴이 용액의 용매에 영향을 받는 문제가 존재했습니다. 이를 해결하기 위해서 계면활성제를 이용해 용해도를 일시적으로 변경 가능한 기술을 개발하였으며 이를 통해서 높은 정밀도를 가지는 패턴 형성 기술을 선보였습니다.
상기 개발된 색선택성을 위한 기술 및 용액 공정을 위한 용해도 변환 공정의 경우 용액 공정을 통한 유기 이미지센서 및 유기 광전기기에 필수적인 기술입니다. 이는 발전하는 현대 유기 광전기기의 성장에 큰 도움이 될 것으로 예상됩니다.

핵심어: 유기 이미지센서, 유기 광다이오드, 유기반도체, 패턴 공정